HHS Public Access

Author manuscript

Nanoscale. Author manuscript; available in PMC 2017 August 14.

Published in final edited form as:

Nanoscale. 2016 August 14; 8(30): 14411–14419. doi:10.1039/c6nr04091h.

Ultra-Small Lipid-Polymer Hybrid Nanoparticles for Tumor-Penetrating Drug Delivery

Diana Dehaini[a,b], **Ronnie H. Fang**[a,b], **Brian T. Luk**[a,b,c], **Zhiqing Pang**[a,d], **Che-Ming J. Hu**[e], **Ashley V. Kroll**[a,b], **Chun Lai Yu**[a], **Weiwei Gao**[a,b], and **Liangfang Zhang**[a,b,c]

Liangfang Zhang: zhang@ucsd.edu

[a]Department of NanoEngineering, University of California, San Diego, La Jolla, CA 92093, USA., Tel: +1-858-246-0999

[b]Moores Cancer Center, University of California, San Diego, La Jolla, CA 92093, USA

[c]Department of Bioengineering, University of California, San Diego, La Jolla, CA 92093, USA

[d]Department of Pharmaceutics, School of Pharmacy, Fudan University, and Key Laboratory of Smart Drug Delivery (Fudan University), Ministry of Education, Shanghai 201203, P. R. China

[e]Institute of Biomedical Sciences, Academia Sinica, Taipei, Taiwan

Abstract

Lipid-polymer hybrid nanoparticles, consisting of a polymeric core coated by a layer of lipids, are a class of highly scalable, biodegradable nanocarriers that have shown great promise in drug delivery applications. Here, we demonstrate the facile synthesis of ultra-small, sub-25 nm lipid-polymer hybrid nanoparticles using an adapted nanoprecipitation approach and explore their utility for targeted delivery of a model chemotherapeutic. The fabrication process is first optimized to produce a monodisperse population of particles that are stable under physiological conditions. It is shown that these ultra-small hybrid nanoparticles can be functionalized with a targeting ligand on the surface and loaded with drug inside the polymeric matrix. Further, the *in vivo* fate of the nanoparticles after intravenous injection is characterized by examining the blood circulation and biodistribution. In a final proof-of-concept study, targeted ultra-small hybrid nanoparticles loaded with the cancer drug docetaxel are used to treat a mouse tumor model and demonstrate improved efficacy compared to a clinically available formulation of the drug. The ability to synthesize a significantly smaller version of the established lipid-polymer hybrid platform can ultimately enhance its applicability across a wider range of applications.

Graphical Abstract

We report on the synthesis of ultra-small lipid-polymer hybrid nanoparticles using a charge-based stabilization method. It is demonstrated that the nanoparticles can be functionalized with targeting ligands as well as loaded with model a chemotherapeutic. Efficacy is evaluated in a mouse xenograft model and compared with a commonly used clinical drug formulation.

Correspondence to: Liangfang Zhang, zhang@ucsd.edu.

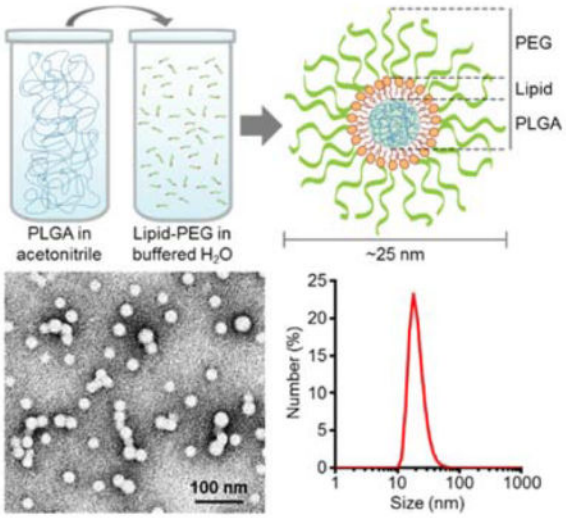

1. Introduction

Nanoparticle technology has facilitated a great deal of improvement in the field of drug delivery over the past several decades.[1, 2] Newer generation nanocarriers have built upon the success of traditional platforms with further optimizations in material, size, and structural properties in order to ultimately improve their therapeutic potential.[3, 4] Lipid-polymer hybrid nanoparticles are one such example, as they combine the merits of liposomes and polymeric nanoparticles,[5] both of which have been extensively evaluated in the clinic.[6, 7] The hybrid nanoparticles comprise of a biodegradable polymeric core surrounded by a lipid layer with a polyethylene glycol (PEG) coating. The hydrophobic nature of the core enables simple encapsulation and delivery of hydrophobic drugs,[5, 8] which typically have poor bioavailability when administered *in vivo* and cannot be used in their free form. Dual loading of two different payloads, including both hydrophobic and hydrophilic drugs within the same particle, has also been demonstrated.[9] Further, the degradability of the particles can be modulated by adjusting polymer properties or employing stimuli-responsive materials, enabling fine-tuned drug release profiles.[10–12] The outer layer provides a biocompatible, stealth coating that enhances residence time in the bloodstream while also acting as a diffusional barrier against drug release.[5, 13] It has been demonstrated that lipid-polymer hybrid nanoparticles are facile to synthesize,[14] and they are also highly scalable, with clinically relevant quantities easily fabricated using fluidic mixing devices.[15, 16] Many different therapeutic and imaging agents have shown improved delivery and efficacy upon formulation inside the hybrid nanoparticles, including chemotherapeutics,[8, 9, 17] nucleic acids,[18, 19] and smaller metallic nanoparticles[20] among many others.

Altering the size of nanoparticles can drastically alter their performance *in vivo* by impacting important parameters such as circulation time and biodistribution.[21] Nanoparticles greater than 200 nm are readily cleared by the liver and spleen, while nanoparticles smaller than approximately 5 nm in size will be filtered by the kidney.[22, 23] There is much debate on the ideal size of nanoparticles for drug delivery, which suggests that optimal sizing may be dependent on both the specific platform in question as well as the intended

application.[21, 24, 25] As an example, delivery of nanoparticles to the brain via systemic injection is particularly difficult due to the blood-brain barrier, but it has been shown that ultra-small particles can experience improved localization to the organ.[26, 27] The influence of nanoparticle size on tumor treatment has been also investigated; particles smaller than 50 nm can more easily penetrate deeper into the center of tumors, where the cancer stem-like cells responsible for controlling tumor proliferation and recurrence are thought to reside.[24, 25, 28, 29] Given the potential benefits, the ability to push the lower limits of size for nanoparticle platforms that have traditionally existed in larger forms is highly desirable.

Here, we demonstrate a facile synthesis scheme for "ultra-small" lipid-polymer hybrid nanoparticles with a final size less than 25 nm (Fig. 1a). Previously reported sizes of hybrid nanoparticles have ranged from 50 nm to greater than 200 nm, and synthesis at the lower range has generally required the fine-tuning of solvent composition, polymer concentration, and lipid-to-polymer ratios.[8] In order to significantly push to lower limits of size, a nanoprecipitation approach employing charge-based polymer stabilization[30] was applied to the hybrid platform for the first time. Overall, the ability to engineer an ultra-small version of the lipid-polymer hybrid nanoparticle has the potential to significantly boost the utility of this already promising platform for a variety of applications, including brain-targeted delivery,[26, 27] deep tumor penetration,[24, 25, 28, 29] and vaccination.[31] In the present study, the stability of the final formulation under different physiologically relevant conditions was confirmed. Further, we were able to introduce cancer targeting functionality as well as encapsulate a chemotherapeutic payload. *In vivo*, both the circulation time and the final biodistribution of the nanoparticles were characterized. Finally, the potential of a folate-functionalized ultra-small hybrid formulation loaded with docetaxel was evaluated for cancer treatment in a mouse xenograft tumor model. The results were compared to those obtained from a clinically used formulation of the same drug, and the targeted ultra-small hybrid nanoparticles exhibited greatly improved inhibition of tumor growth.

2. Materials and methods

2.1 Ultra-small lipid-polymer hybrid nanoparticle preparation

Ultra-small lipid-polymer hybrid nanoparticles were prepared using a modified nanoprecipitation process. 1,2-distearoyl-sn-glycero-3-phosphoethanolamine-N-[methoxy(polyethylene glycol)-2000] (DSPE-PEG_{2000}; Avanti Polar Lipids) dissolved in chloroform was deposited in a glass vial, and the solvent was allowed to evaporate. The resulting thin film was then hydrated in water containing Tris-HCl at pH 8 (Affymetrix). Carboxylic acid-terminated poly(lactic-*co*-glycolic acid) (PLGA-COOH; 0.67 dL/g, 50:50 ratio; Lactel Absorbable Polymers) dissolved at 1 mg/mL in acetonitrile was added rapidly to the DSPE-PEG_{2000}-containing aqueous phase. Particles were purified by washing with water 3 times using 100 kDa MWCO Amicon centrifugal filters (EMD Millipore). Size and zeta potential were measured by dynamic light scattering (DLS) using a Malvern ZEN 3600 Zetasizer. Given the ultra-small size of the nanoparticles, number distribution was reported to most accurately reflect the actual size of the nanoparticles as confirmed by imaging experiments. Transmission electron microscopy (TEM) was conducted by depositing nanoparticle samples on a glow-discharged, carbon-coated 400-mesh copper grid (Electron

Microscopy Sciences). The grid was then washed using distilled water and stained with 1 wt % uranyl acetate (Electron Microscopy Sciences). Imaging was carried out on a Zeiss Libra 120 PLUS EF-TEM transmission electron microscope. Bare PLGA cores were prepared similarly to the hybrid nanoparticles, but without DSPE-PEG_{2000} in the aqueous phase.

2.2 Stability studies

Stability of the ultra-small hybrid nanoparticles was analyzed in 10 mM Tris-HCl at pH 8, phosphate buffered saline (PBS), and fetal bovine serum (FBS). For stability in 10 mM Tris-HCl, hybrid nanoparticles, as well as PLGA cores, were synthesized as described above at a final polymer concentration of 1 mg/mL. To test the stability in 1X PBS, nanoparticles samples at 2 mg/mL were added to an equal volume of 2X PBS. The size of the samples in both 10 mM Tris-HCl and 1X PBS were measured by DLS daily for 8 days, at which point they were measured every two days until day 14. For the serum stability study, an absorbance-based approach was employed.[14, 32] 100% FBS was concentrated to 2X protein concentration using 10 kDa MWCO Amicon centrifugal filters (EMD Millipore). An equal volume of either 10 mM Tris-HCl or the FBS concentrate was then added to nanoparticle suspensions at 2 mg/mL in 10 mM Tris-HCl aliquoted into the wells of a clear 96-well plate (Corning). Absorbance of the samples were measured in a Tecan Infinite M200 plate reader at 560 nm, a wavelength previously established to detect for the formation of aggregates.[14] Signals were adjusted by subtracting the reading of equivalent blank solutions without nanoparticles at the same wavelength.

2.3 Targeting studies

Hybrid nanoparticles targeting the folate receptor were synthesized by replacing 10 wt% of the DSPE-PEG_{2000} in the optimized formulation with folate-conjugated DSPE-PEG_{2000} (Nanocs). To evaluate the targeted formulation *in vitro*, KB cells (CCL17; American Type Culture Collection) were cultured in RPMI-1640 media (Mediatech). At 24 hours prior to the start of the experiment, the media was changed to folate-free RPMI-1640 (Life Technologies). Fluorescently labeled hybrid nanoparticles, either non-targeted or targeted, were fabricated by the addition of 0.1 wt% 1,13-dioctadecyl-3,3,33,33-tetramethylindodicarbocyanine, 4-chlorobenzenesulfonate salt (DiD; Biotium) to the organic phase during synthesis. The DiD dye, hydrophobic in nature, naturally associates with the PLGA core material during self-assembly. The particles were added to the KB cells at a final concentration of 0.25 mg/mL and allowed to incubate at 37 °C for 30 minutes. The cells were then washed 3 times with 1X PBS and finally suspended in VECTASHIELD Antifade mounting media with DAPI (Vector Laboratories). Fluorescent imaging was performed on a KEYENCE BZ-X710 fluorescence microscope with a 20X objective using both the DAPI and Cy5 filters with consistent exposure times. The two channels were overlaid and all images were subject to the same brightness and contrast adjustments. For flow cytometric analysis, cells were incubated with nanoparticles the same as above, and then detached using trypsin-EDTA (Life Technologies). The collected cells were washed 3 times with 1X PBS and measured on a Becton Dickinson FACSCanto II flow cytometer using the red laser and Alexa Fluor 647 filter. Data analysis to find the mean fluorescence intensity of each sample was performed using Treestar Flowjo software.

To examine the *in vivo* tumor penetration, 6-week-old immunocompromised female nu/nu (nude) mice (obtained from a breeding colony at the University of California, San Diego) were subcutaneously implanted with 1×10^6 KB cells using 50% Matrigel (BD Biosciences) in the hind flank region. All animal experiments were performed in accordance with NIH guidelines and approved by the Institutional Animal Care and Use Committee (IACUC) of the University of California, San Diego. After 3 weeks, mice were injected intravenously via the tail vein with 200 μL of 15 mg/mL DiD-labeled hybrid nanoparticles, either non-targeted or targeted. The mice were euthanized after 24 hours and the tumors were extracted. Tumors were flash frozen in Tissue-Tek O.C.T. compound (Sakura Finetek) and sectioned for histological analysis. FITC-conjugated anti-mouse CD31 (Clone: MEC13.3; Biolegend) was used to label tumor vasculature. Images were taken on a KEYENCE BZ-X710 fluorescence microscope with a 10X objective using both the GFP and Cy5 filters with consistent exposure times. The two channels were overlaid and all images were subject to the same brightness and contrast adjustments. Intensity analysis was conducted using ImageJ, and each set of data was normalized such that the maximum mean was 100%.

2.4 Docetaxel loading and cytotoxicity

The chemotherapeutic docetaxel (Biotang) was loaded into the ultra-small hybrid nanoparticles by physical encapsulation. Drug was dissolved with PLGA in the organic phase, and the synthesis proceeded as described above. Particles were washed 3 times with 100 kDa MWCO Amicon centrifugal filters to remove unencapsulated docetaxel. In order to quantify the amount of drug loaded, the purified nanoparticles were lyophilized and dissolved in acetonitrile to release the drug. Samples were analyzed on a PerkinElmer Series 200 high performance liquid chromatography (HPLC) system using a C18 analytical column (Brownlee) with a mobile phase of 50:50 water to acetonitrile and a detection wavelength of 230 nm. Different weight ratios of drug to polymer, ranging from 0% to 20% were tested in order to optimize drug loading. Known concentrations of docetaxel were used to generate a standard curve. Drug release over time was characterized by dialyzing samples against 1X PBS in 10 kDa MWCO Slide-A-Lyzer MINI dialysis cups (Thermo Scientific). The amount of drug retained in the nanoparticle samples was assessed at 0, 1, 2, 4, 6, 12, 24, 48, and 72 hours. Samples were collected, lyophilized, and then analyzed by HPLC as described above.

Cytotoxicity of the nanoparticles was evaluated by seeding KB cells at 15,000 per well in a 96-well plate. Serially diluted solutions of docetaxel-loaded ultra-small hybrids or Taxotere (Sanofi), giving final drug concentrations starting at 100 ng/mL, were incubated with the cells for a period of 72 hours. After drug incubation, the wells were washed with 1X PBS and a 3-(4,5-dimethylthiazol-2-yl)-2,5-diphenyltetrazolium bromide (MTT) assay was used to quantify cell viability. The MTT reagent (Invitrogen) was incubated with the cells for 4 hours, after which the solution was carefully aspirated and the precipitated crystals dissolved using dimethyl sulfoxide. Absorbance was read at 560 nm on a Tecan Infinite M200 plate reader. Cells lysed with 0.5% Triton-X 100 (Sigma Aldrich) in PBS and untreated cells were used to establish 0% and 100% viability, respectively. IC_{50} values were determined by fitting the data using a dose-response inhibition curve in Graphpad Prism.

2.5 *In vivo* circulation and biodistribution

To study the circulation time of ultra-small hybrids *in vivo*, DiD-labeled nanoparticles, 200 μL at 10 mg/mL, were injected via the tail vein of 6-week-old male CD1 mice (Harlan Laboratories). Immunocompetent mice were used to best approximate the *in vivo* fate of the nanoparticles. Approximately 100 μL of blood was collected by cheek puncture via the submandibular vein at the following timepoints: right after injection and 0.33, 1, 3, 8, 24, 48, and 72 hours. Samples were diluted by 10 times in water and the fluorescence quantified on a Tecan Infinite M200 plate reader at excitation and emission wavelengths of 630 nm and 670 nm, respectively. Blank signal from diluted blood was subtracted from all measurements, and the data was normalized to the signal from the timepoint right after injection. The data was first fitted using a decay regression model in Graphpad Prism, and the program was used to interpolate the time corresponding to 50% clearance. To calculate the elimination half-life, the normalized signal was transformed using natural log, and the resulting data was fitted using a linear regression curve. Elimination half-life was calculated as $t_{1/2} = 1n(2) / \beta$, where β is the negative slope obtained from the fit.

To study the biodistribution of ultra-small hybrid nanoparticles, a DiD-labeled formulation was administered via the tail vein at 10 mg/mL in a volume of 200 μL. At 24 hours after injection, the mice were euthanized and subject to whole body perfusion with 1X PBS. Afterwards, the heart, lungs, spleen, kidneys, and liver were harvested and homogenized using a Biospec Mini-Beadbeater-16. Organ fluorescence values were obtained by measuring the homogenate on a Tecan Infinite M200 plate reader at excitation and emission wavelengths of 630 nm and 670 nm, respectively. Background signal was subtracted using organ samples collected from mice not injected with nanoparticles.

2.6 *In vivo* tumor treatment efficacy

6-week-old immunocompromised female nude mice were subcutaneously implanted with 1×10^6 KB cells using 50% Matrigel in the hind flank region. At the beginning of week 3, corresponding to 14 days after implantation, tumors were palpable and treatment was initiated with the following: blank solution, non-targeted ultra-small hybrid nanoparticles, targeted ultra-small hybrid nanoparticles, and Taxotere. All drug-containing formulations were administered at 4 mg/kg of docetaxel. Treatments were administered twice per week on weeks 3 and 5 for a total of 4 treatments. Tumor dimensions were measured every other day and the total volume was calculated by the equation $V = (width^2 \times length)/2$, where width and length represent the smallest and largest dimensions, respectively, in the same plane as the skin surface. Body weight was also monitored every other day. Mice were euthanized when their tumor volume exceeded a predetermined threshold of 2,000 mm^3.

3. Results and discussion

3.1 Fabrication and optimization of formulation parameters

Ultra-small lipid-polymer hybrid nanoparticles were fabricated using a modified nanoprecipitation reaction. Carboxylic acid-terminated poly(lactic-*co*-glycolic acid) (PLGA-COOH) was dissolved in acetonitrile and added into an aqueous phase buffered with Tris-HCl at pH 8 containing polyethylene glycol (PEG)-conjugated lipids (lipid-PEG). After

ultrafiltration, the resulting nanoparticles were characterized by dynamic light scattering (DLS) (Fig. 1b–d). According to the measurements, hybrid nanoparticles were several nanometers larger than the bare PLGA cores, and the zeta potential increased significantly from less than −50 mV to greater than −10 mV when the uncharged lipid-PEG layer was introduced. The data suggests successful surface functionalization of the bare PLGA cores with a layer of lipid-PEG. Further, the number-based size distribution curve obtained from DLS showed a tight grouping around the average nanoparticle size. Visual observation using transmission electron microscopy (TEM) of the hybrid nanoparticles negatively stained with uranyl acetate confirmed that there was a monodisperse population less than 25 nm in size (Fig. 1e).

To optimize the buffer conditions for size minimization, PLGA cores were prepared with varying amounts of buffer in the aqueous phase, ranging from 0 mM to 20 mM Tris-HCl at pH 8 (Fig. 2a). The smallest nanoparticle cores at just over 20 nm in size were observed when using 10 mM Tris-HCl, and this buffering condition was selected for further studies. Minimization at an intermediate concentration suggests that sufficient buffering capacity and charge screening represent two opposing factors affecting the final size. Next, the amount of lipid-PEG necessary for stabilization of the PLGA cores under physiological conditions was assessed (Fig. 2b). Nanoparticles were synthesized in 10 mM Tris-HCl at pH 8 with lipid-PEG to PLGA weight ratios ranging 0% to 40%, and the solutions were subsequently adjusted to 1X phosphate buffered saline (PBS). Bare cores with no lipid-PEG coating immediately aggregated upon introduction of PBS due to charge screening, an expected outcome given that the particles rely solely on charge stabilization. With increasing amounts of lipid-PEG, the particles exhibited a trend of diminishing size increase after adjusting to 1X PBS. Size minimization occurred approximately at a 30% ratio, and a conservative ratio of 40% lipid-PEG to PLGA was used for further studies. The amount of lipid-PEG necessary to stabilize a given amount of ultra-small PLGA cores was higher than that previously reported for larger hybrid nanoparticle formulations,[5] a difference that reflects the increased surface area of the ultra-small particles.

3.2 Nanoparticle stability

The stability over time of the final ultra-small hybrid formulation was evaluated over time in both 10 mM Tris-HCl and PBS (Fig. 3a). Bare PLGA cores immediately aggregated in PBS to over 1 μm but stayed stable in water over a period of two weeks. In contrast, the hybrid nanoparticle formulation exhibited no increase in size for the duration of the study under both conditions, demonstrating their ability to be stored long-term in solution. Stability of the nanoparticles in 100% fetal bovine serum (FBS) was analyzed using an absorbance-based method (Fig. 3b).[32] Upon addition of FBS to the bare PLGA cores, a marked increase in absorbance was observed, reflecting increased scattering by newly formed particle aggregates. An increase in absorbance was not observed for ultra-small hybrid nanoparticles subjected to the same treatment, indicating particle stability in the presence of serum proteins. Taken together, the stability characteristics of the final hybrid formulation indicated their suitability for further *in vitro* and *in vivo* evaluation.

3.3 Introduction of targeting functionality

The ability to introduce targeting functionality onto the surface of nanoparticles can help to facilitate more efficient localization to a site of interest.[33–35] In order to demonstrate this for ultra-small hybrid nanoparticles, we used folate, a classical targeting ligand that takes advantage of the fact that many cancers overexpress the folate receptor.[36, 37] Folate-functionalized nanoparticles were fabricated by substituting 10% of the lipid-PEG in the optimized hybrid nanoparticle formulation with lipid-PEG pre-conjugated with folate. The targeting property of this formulation was tested on KB cells, which are known to overexpress the folate receptor (Fig. 4a,b).[38] Fluorescent dye-labeled ultra-small hybrids with or without folate functionality, respectively referred to as targeted or non-targeted formulations, were incubated with the cells, and fluorescence microscopy revealed significantly higher uptake for the targeted formulation. This was further confirmed by flow cytometry, as the mean fluorescence intensity indicated that the targeted formulation had approximately 3 times the uptake compared to the non-targeted formulation. For cells initially blocked with free folate, the level of uptake for the targeted formulation was reduced to that of the non-targeted, indicating that the increased uptake was receptor specific.

Next, we examined the ability of the ultra-small hybrid nanoparticles to penetrate into tumors after systemic administration in a folate receptor-overexpressing murine xenograft tumor model. The same KB cell line used for the *in vitro* targeting evaluation was grown subcutaneously in nude mice, and fluorescently labeled targeted or non-targeted hybrid nanoparticles were administered via the tail vein (Fig. 4c). After 24 hours, the mice were euthanized for histological analysis of the tumors. The non-targeted formulation was shown to localize near areas staining positive for the endothelial marker CD31, which was used to delineate tumor vasculature.[39] In contrast, the targeted hybrid nanoparticles were found much deeper within the tumor and further away from the vasculature. Image analysis corroborated these observations quantitatively, as the signal of the non-targeted formulation coincided with the vasculature signal, whereas the signal of the targeted formulation displayed high intensity throughout (Fig. 4d–g). The difference demonstrates that the additional folate functionality of the targeted nanoparticles can be used to improve tumor penetration by enhancing retention via receptor-specific interactions. Regarding the low presence of non-targeted nanoparticles away from the vasculature, it has been discussed previously that small nanoparticles can penetrate deeper into tumors due to their size, but without a targeting ligand they are also subject to rapid clearance by the same mechanism.[29] The ability to target payloads to all areas of a tumor has important implications for treatment and can potentially be used to more effectively destroy cancer stem cells.[40]

3.4 Drug loading and cytotoxicity

The drug loading capacity of the ultra-small hybrid nanoparticles was evaluated using docetaxel, a hydrophobic chemotherapeutic commonly used to treat a variety of cancer types in the clinic.[41] In order to optimize the loading of docetaxel into the nanoparticles, drug input to PLGA weight ratios ranging from 0% to 20% were tested (Fig. 5a). After removal of free drug by ultrafiltration, the drug loading was quantified by high performance liquid chromatography (HPLC). There was a trend of increasing amounts of loaded docetaxel with

increasing initial inputs that remained fairly linear up to 15% drug input. Maximal loading was observed at 20%, and it should be noted that, at higher concentrations, drug-loaded particles were not stable and precipitated out of solution. Thus, a drug-loaded formulation employing the 20% input with a final drug loading of approximately 2% was used for further studies. Next, a drug release study was conducted by dialyzing the docetaxel-loaded ultra-small particles against 1X PBS (Fig. 5b). An initial burst was observed during the first 12 hours, with approximately 50% of the docetaxel released during this period. By the conclusion of the study at 72 hours, a large majority of the drug had been released. Finally, the activity of the drug-loaded formulation was tested by assessing the cytotoxicity of the particles *in vitro* (Fig. 5c). KB cells were incubated for 72 hours with either Taxotere, a clinically used formulation of docetaxel, or drug-loaded ultra-small hybrid nanoparticles at equivalent drug concentrations. The cytotoxicity profile of the two formulations were nearly identical, and IC_{50} values were calculated to be 731 pg/mL and 624 pg/mL for the ultra-small hybrid and Taxotere formulations, respectively. This finding suggests that the activity of the drug remained largely unaltered after being loaded into the hybrid nanoparticles. It should be noted that lipid-polymer hybrid nanoparticles alone when used in the quantities involved in this study have previously been demonstrated to not exhibit toxicity.[42]

3.5 *In vivo* circulation and biodistribution

The fate of ultra-small hybrid nanoparticles after intravenous injection was evaluated. First, the blood circulation in mice was studied after administration of fluorescently labeled nanoparticles via the tail vein (Fig. 6a). Blood was drawn immediately after injection and at timepoints of 0.33, 1, 3, 8, 24, 48, and 72 hours. According to the data, 50% of the particles were cleared by 3.4 hours, and approximately 10% of particles were remaining at 24 hours. Further analysis using a two-compartment model yielded an elimination half-life of approximately 11.5 hours. The ability of the ultra-small hybrid formulation to circulate for an extended period of time can be attributed to the stabilizing properties of the lipid-PEG outer layer, which prevents non-specific protein interactions that facilitate nanoparticle clearance *in vivo*. This is in stark contrast to bare PLGA cores, which are known to exhibit extremely short blood circulation times.[32]

Next, a biodistribution study was conducted to study organ-level localization of the nanoparticles after intravenous injection (Fig. 6b,c). Mice were administered with fluorescently labeled ultra-small hybrid nanoparticles. After 24 hours, the mice were euthanized, and the heart, lungs, spleen, kidneys, and liver were collected. After mechanical homogenization, the signal from each organ was quantified. It was shown that the highest absolute amount of fluorescence was present in the liver, an expected outcome given that the organ has been widely shown to play an important role in nanoparticle clearance.[22] There were relatively low amounts of signal in the other organs tested. Notably, the signal in the lungs was very low, a desirable finding given the potential toxicity associated with over-accumulation.[43, 44] The results observed are in line with previously reported data for similarly structured nanoparticles.[13, 32, 45]

3.6 *In vivo* tumor treatment efficacy

Given the stability of the ultra-small hybrid nanoparticles both *in vitro* and *in vivo*, their capacity for drug loading, and their ability to be functionalized with an active targeting ligand, we tested their potential for cancer treatment in a murine xenograft tumor model. KB cells were implanted in nude mice and allowed to develop into palpable tumors over the course of two weeks. Afterwards, docetaxel-loaded ultra-small hybrids, both targeted and non-targeted, were administered a total of 4 times (twice per week on weeks 3 and 5) at a dosage of 4 mg/kg (Fig. 7a–c). Taxotere, at the same drug dosage, as well as blank solution were used as controls. As expected, the tumors in mice treated with blank solution continued to progress, with a median survival of 38 days after tumor implantation. Both the non-targeted ultra-small formulation and Taxotere showed similar growth kinetics, showing moderate control of tumor growth and extending median survival to 44 and 46 days, respectively. The targeted ultra-small formulation performed the best, significantly suppressing tumor growth, and more than half of the mice were still alive at 64 days after tumor challenge. As an indicator of global health, body weights were monitored over the course of the study. The body weight measurements from the treatment groups were not significantly different from those treated with blank solution, suggesting that it may be possible to raise the dosing in future studies. It should be noted that the docetaxel dosage used in the present study is lower than previously determined values for the maximum tolerated dose of the Taxotere formulation.[46, 47] The ability to generate a targeted ultra-small hybrid nanoparticle formulation that significantly outperforms a clinically used formulation highlights the benefit of the platform for tumor treatment applications and suggests that further study may be warranted along these lines.

4. Conclusion

In conclusion, we have demonstrated the fabrication and application of ultra-small lipid-polymer hybrid nanoparticles under 25 nm in size. A simple, charge-based stabilization strategy was employed for the synthesis of a monodisperse population of these particles, which were significantly smaller than previously reported lipid-polymer hybrids. It was shown that the particles retained the advantageous properties of the hybrid nanoparticle platform, including excellent stability *in vitro* and *in vivo*, drug loading capability, and facile incorporation of targeting functionality. Targeted ultra-small hybrids demonstrated effective localization to regions deep within tumors, and, when loaded with the chemotherapeutic docetaxel, were able to outperform a clinically used formulation of the drug. Given that these ultra-small hybrid nanoparticles are fabricated from FDA-approved materials and employ a facile synthesis scheme, they appear primed for translation, although further studies on the scale-up of this specific formulation are warranted. Ultimately, the addition of an ultra-small version to the size repertoire of hybrid nanoparticles helps to further boost the utility of the platform and may provide a means of improving the therapeutic profile of drug payloads across a wide range of different applications.

Acknowledgments

This work is supported by the National Science Foundation Grant DMR-1505699 and the National Institute of Diabetes and Digestive and Kidney Diseases of the National Institutes of Health under Award Number R01DK095168.

Notes and references

1. Brannon-Peppas L, Blanchette JO. Adv Drug Deliv Rev. 2004; 56:1649–1659. [PubMed: 15350294]
2. Wagner V, Dullaart A, Bock AK, Zweck A. Nat Biotechnol. 2006; 24:1211–1217. [PubMed: 17033654]
3. Wang AZ, Langer R, Farokhzad OC. Annu Rev Med. 2012; 63:185–198. [PubMed: 21888516]
4. Farokhzad OC, Langer R. ACS Nano. 2009; 3:16–20. [PubMed: 19206243]
5. Zhang L, Chan JM, Gu FX, Rhee JW, Wang AZ, Radovic-Moreno AF, Alexis F, Langer R, Farokhzad OC. ACS Nano. 2008; 2:1696–1702. [PubMed: 19206374]
6. Kamaly N, Xiao Z, Valencia PM, Radovic-Moreno AF, Farokhzad OC. Chem Soc Rev. 2012; 41:2971–3010. [PubMed: 22388185]
7. Pattni BS, Chupin VV, Torchilin VP. Chem Rev. 2015; 115:10938–10966. [PubMed: 26010257]
8. Chan JM, Zhang L, Yuet KP, Liao G, Rhee JW, Langer R, Farokhzad OC. Biomaterials. 2009; 30:1627–1634. [PubMed: 19111339]
9. Aryal S, Hu CMJ, Fu V, Zhang L. J Mater Chem. 2012; 22:994–999.
10. Cheng R, Meng F, Deng C, Klok HA, Zhong Z. Biomaterials. 2013; 34:3647–3657. [PubMed: 23415642]
11. Makadia HK, Siegel SJ. Polymers (Basel). 2011; 3:1377–1397. [PubMed: 22577513]
12. Clawson C, Ton L, Aryal S, Fu V, Esener S, Zhang L. Langmuir. 2011; 27:10556–10561. [PubMed: 21806013]
13. Gref R, Domb A, Quellec P, Blunk T, Muller RH, Verbavatz JM, Langer R. Adv Drug Deliv Rev. 1995; 16:215–233. [PubMed: 25170183]
14. Fang RH, Aryal S, Hu CM, Zhang L. Langmuir. 2010; 26:16958–16962. [PubMed: 20961057]
15. Valencia PM, Farokhzad OC, Karnik R, Langer R. Nat Nanotechnol. 2012; 7:623–629. [PubMed: 23042546]
16. Karnik R, Gu F, Basto P, Cannizzaro C, Dean L, Kyei-Manu W, Langer R, Farokhzad OC. Nano Lett. 2008; 8:2906–2912. [PubMed: 18656990]
17. Aryal S, Hu CMJ, Zhang L. Mol Pharm. 2011; 8:1401–1407. [PubMed: 21696189]
18. Hasan W, Chu K, Gullapalli A, Dunn SS, Enlow EM, Luft JC, Tian SM, Napier ME, Pohlhaus PD, Rolland JP, DeSimone JM. Nano Lett. 2012; 12:287–292. [PubMed: 22165988]
19. Su XF, Fricke J, Kavanagh DG, Irvine DJ. Mol Pharm. 2011; 8:774–787. [PubMed: 21417235]
20. Kong SD, Sartor M, Hu CM, Zhang W, Zhang L, Jin S. Acta Biomater. 2013; 9:5447–5452. [PubMed: 23149252]
21. Yoo JW, Chambers E, Mitragotri S. Curr Pharm Des. 2010; 16:2298–2307. [PubMed: 20618151]
22. Alexis F, Pridgen E, Molnar LK, Farokhzad OC. Mol Pharm. 2008; 5:505–515. [PubMed: 18672949]
23. Blanco E, Shen H, Ferrari M. Nat Biotechnol. 2015; 33:941–951. [PubMed: 26348965]
24. Tang L, Gabrielson NP, Uckun FM, Fan TM, Cheng J. Mol Pharm. 2013; 10:883–892. [PubMed: 23301497]
25. Ni D, Ding H, Liu S, Yue H, Bao Y, Wang Z, Su Z, Wei W, Ma G. Small. 2015; 11:2518–2526. [PubMed: 25678130]
26. Bramini M, Ye D, Hallerbach A, Raghnaill MN, Salvati A, Aberg C, Dawson KA. ACS Nano. 2014; 8:4304–4312. [PubMed: 24773217]
27. Jo DH, Kim JH, Lee TG, Kim JH. Nanomedicine. 2015; 11:1603–1611. [PubMed: 25989200]
28. Rao W, Wang H, Han J, Zhao S, Dumbleton J, Agarwal P, Zhang W, Zhao G, Yu J, Zynger DL, Lu X, He X. ACS Nano. 2015; 9:5725–5740. [PubMed: 26004286]

29. Tang L, Yang X, Yin Q, Cai K, Wang H, Chaudhury I, Yao C, Zhou Q, Kwon M, Hartman JA, Dobrucki IT, Dobrucki LW, Borst LB, Lezmi S, Helferich WG, Ferguson AL, Fan TM, Cheng J. Proc Natl Acad Sci USA. 2014; 111:15344–15349. [PubMed: 25316794]
30. Reisch A, Runser A, Arntz Y, Mely Y, Klymchenko AS. ACS Nano. 2015; 9:5104–5116. [PubMed: 25894117]
31. Reddy ST, van der Vlies AJ, Simeoni E, Angeli V, Randolph GJ, O'Neil CP, Lee LK, Swartz MA, Hubbell JA. Nat Biotechnol. 2007; 25:1159–1164. [PubMed: 17873867]
32. Hu CM, Zhang L, Aryal S, Cheung C, Fang RH, Zhang L. Proc Natl Acad Sci USA. 2011; 108:10980–10985. [PubMed: 21690347]
33. Dehaini D, Fang RH, Zhang L. Bioeng Transl Med.
34. Bazak R, Houri M, El Achy S, Kamel S, Refaat T. J Cancer Res Clin Oncol. 2015; 141:769–784. [PubMed: 25005786]
35. Hu CM, Kaushal S, Tran Cao HS, Aryal S, Sartor M, Esener S, Bouvet M, Zhang L. Mol Pharm. 2010; 7:914–920. [PubMed: 20394436]
36. Sudimack J, Lee RJ. Adv Drug Deliv Rev. 2000; 41:147–162. [PubMed: 10699311]
37. Oyewumi MO, Yokel RA, Jay M, Coakley T, Mumper RJ. J Control Release. 2004; 95:613–626. [PubMed: 15023471]
38. Reddy JA, Haneline LS, Srour EF, Antony AC, Clapp DW, Low PS. Blood. 1999; 93:3940–3948. [PubMed: 10339503]
39. Wang D, Stockard CR, Harkins L, Lott P, Salih C, Yuan K, Buchsbaum D, Hashim A, Zayzafoon M, Hardy RW, Hameed O, Grizzle W, Siegal GP. Biotech Histochem. 2008; 83:179–189. [PubMed: 18846440]
40. Vinogradov S, Wei X. Nanomedicine (Lond). 2012; 7:597–615. [PubMed: 22471722]
41. Earhart RH. Semin Oncol. 1999; 26:8–13. [PubMed: 10604262]
42. Wang AZ, Yuet K, Zhang L, Gu FX, Huynh-Le M, Radovic-Moreno AF, Kantoff PW, Bander NH, Langer R, Farokhzad OC. Nanomedicine (Lond). 2010; 5:361–368. [PubMed: 20394530]
43. Card JW, Zeldin DC, Bonner JC, Nestmann ER. Am J Physiol Lung Cell Mol Physiol. 2008; 295:L400–411. [PubMed: 18641236]
44. Xie G, Sun J, Zhong G, Shi L, Zhang D. Arch Toxicol. 2010; 84:183–190. [PubMed: 19936708]
45. Jokerst JV, Lobovkina T, Zare RN, Gambhir SS. Nanomedicine (Lond). 2011; 6:715–728. [PubMed: 21718180]
46. Vanhoefer U, Cao S, Harstrick A, Seeber S, Rustum YM. Ann Oncol. 1997; 8:1221–1228. [PubMed: 9496387]
47. Desai N, Trieu V, Soon-Shiong P, Hawkins M. Cancer Res. 2005; 65:336–337.

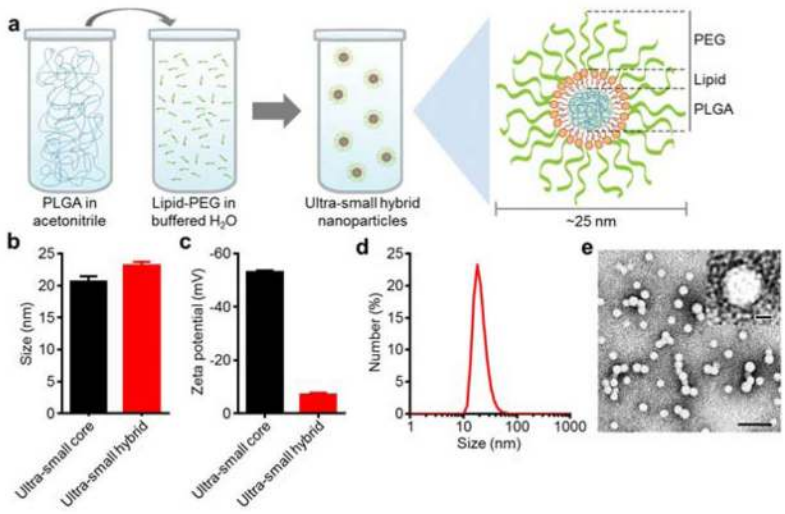

Fig. 1.

Schematic of synthesis and physicochemical characterization of ultra-small lipid-polymer hybrid nanoparticles. (a) Schematic displaying the process for fabricating ultra-small hybrid nanoparticles. Poly(lactic-*co*-glycolic acid) (PLGA) dissolved in acetonitrile is added to a buffered aqueous solution containing lipid-PEG, resulting in the formation of sub-25 nm nanoparticles with a core-shell structure. (b) Number-weighted size measurements of ultra-small PLGA cores and ultra-small hybrid nanoparticles (n = 3; mean ± SD). (c) Zeta potential of ultra-small PLGA cores and ultra-small hybrid nanoparticles (n = 3; mean ± SD). (d) Number-based size distribution of a representative ultra-small hybrid nanoparticle sample. (e) Transmission electron micrograph of ultra-small hybrid nanoparticles (scale bar = 100 nm). Inset shows a single particle (scale bar = 10 nm).

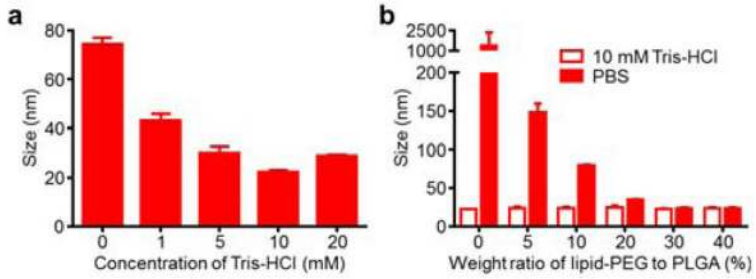

Fig. 2.

Optimization of ultra-small hybrid nanoparticle fabrication. (a) Size measurements of PLGA cores precipitated into different concentrations of Tris-HCl buffer at pH 8 (n = 3; mean ± SD). (b) Size measurements of hybrid nanoparticles synthesized at varying lipid-PEG to PLGA weight ratios (n = 3; mean ± SD). Measurements were taken after synthesis in 10 mM Tris-HCl at pH 8 and after adjusting to 1X PBS (pH 7.4).

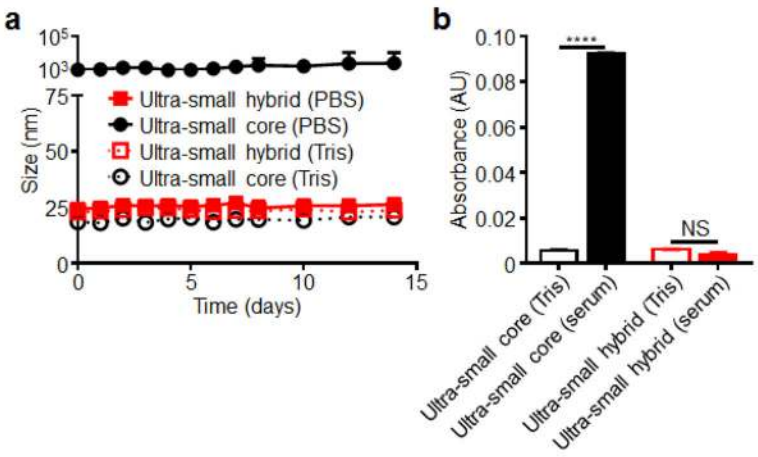

Fig. 3.

Ultra-small hybrid nanoparticle stability studies. (a) Size measurements of ultra-small hybrid nanoparticles and ultra-small PLGA cores over the course of 2 weeks in both 10 mM Tris-HCl at pH 8 and 1X PBS (n = 3; mean ± SD). (b) Absorbance at 560 nm of ultra-small hybrid nanoparticles and ultra-small PLGA cores both in 10 mM Tris-HCl at pH 8 and after adjusting to 100% fetal bovine serum (n = 3; mean ± SD). Background signal was subtracted using corresponding blank solutions with no nanoparticles. ****P<0.0001, NS = not significant, Student's t-test.

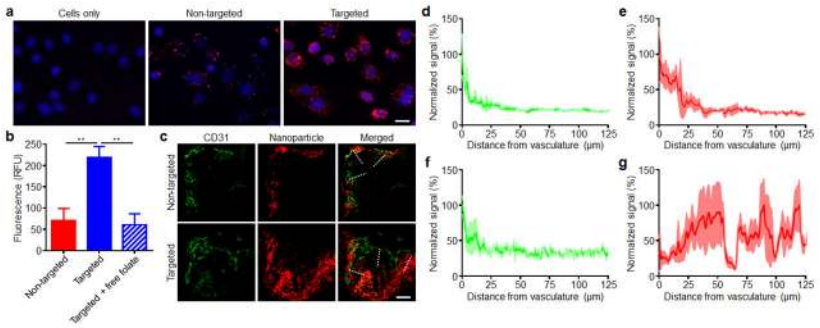

Fig. 4.

Introduction of targeting functionality onto ultra-small hybrid nanoparticles. (a) Fluorescent microscopy visualization of KB cells incubated with fluorescent dye-labeled non-targeted or folate receptor-targeted ultra-small hybrid nanoparticles (red: nanoparticles, blue: cell nuclei; scale bare = 20 μm). (b) Mean fluorescent intensities as quantified by flow cytometry of KB cells incubated with either non-targeted ultra-small hybrid nanoparticles, targeted hybrid nanoparticles, or targeted hybrid nanoparticles with KB cells blocked with free folate (n = 3; mean ± SD). (c) Fluorescent microscopy visualization of histological sections from xenograft KB tumors of mice administered with either fluorescent dye-labeled non-targeted or targeted ultra-small hybrid nanoparticles (red: nanoparticles, green: tumor vasculature; scale bare = 100 μm). (d–g) Normalized fluorescent signal within the tumors of mice administered with non-targeted hybrids (d, vasculature; e, nanoparticles) or targeted hybrids (f, vasculature; g, nanoparticles) as sampled by the dashed lines on the merged images in (c) (n = 3; mean ± SEM). The direction of sampling went from the outside of the tumor towards the center. $^{**}P<0.01$, Student's *t*-test.

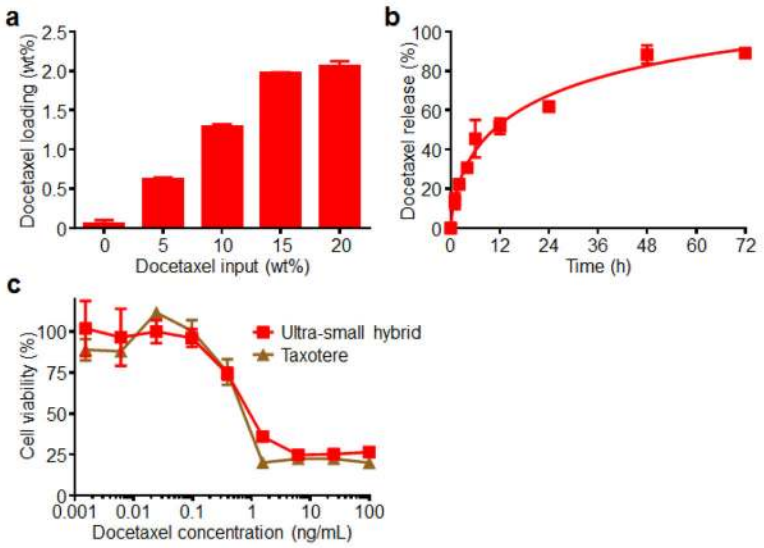

Fig. 5.

Drug loading and characterization of ultra-small hybrid nanoparticles. (a) Drug loading quantification of hybrid nanoparticles fabricated at increasing docetaxel input to PLGA weight ratios (n = 3; mean ± SD). (b) Cumulative release profile of docetaxel-loaded ultra-small hybrid nanoparticles with 2 wt% docetaxel loading over the course of 72 hours in 1X PBS (n = 3; mean ± SD). (c) Cell viability of KB cells treated with either docetaxel-loaded ultra-small hybrid nanoparticles or Taxotere for 72 hours (n = 3; mean ± SD). Samples were normalized according to lysed cell and untreated controls.

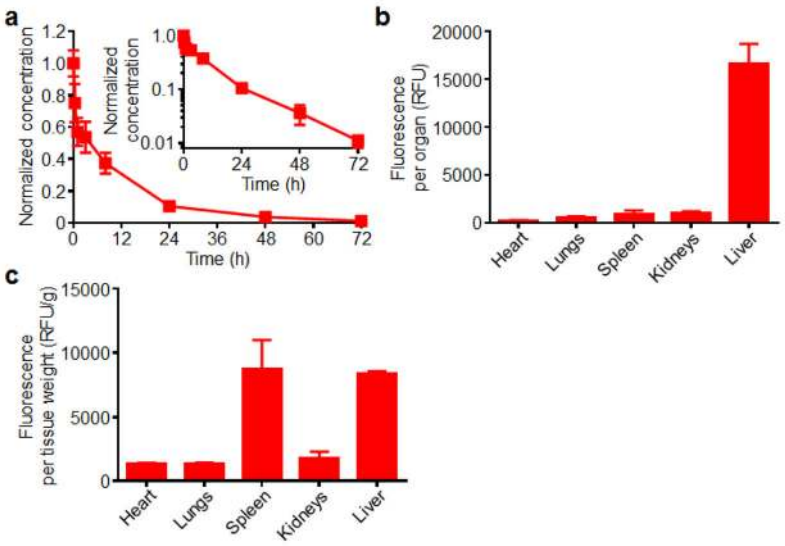

Fig. 6.

In vivo characterization of ultra-small hybrid nanoparticles. (a) Circulation time of fluorescent dye-labeled ultra-small hybrid nanoparticles after intravenous administration (n = 6; mean ± SD). Blood samples were collected at designated timepoints and measured for fluorescence intensities. Signals were normalized according to the first collected sample right after injection. Inset shows the data on a semi-log plot. (b) Biodistribution of fluorescent dye-loaded ultra-small hybrid nanoparticles 24 hours after intravenous administration (n = 3; mean ± SD). Fluorescent signal was measured from homogenized organs after whole body perfusion. (c) The biodistribution data in (b) normalized by organ weight.

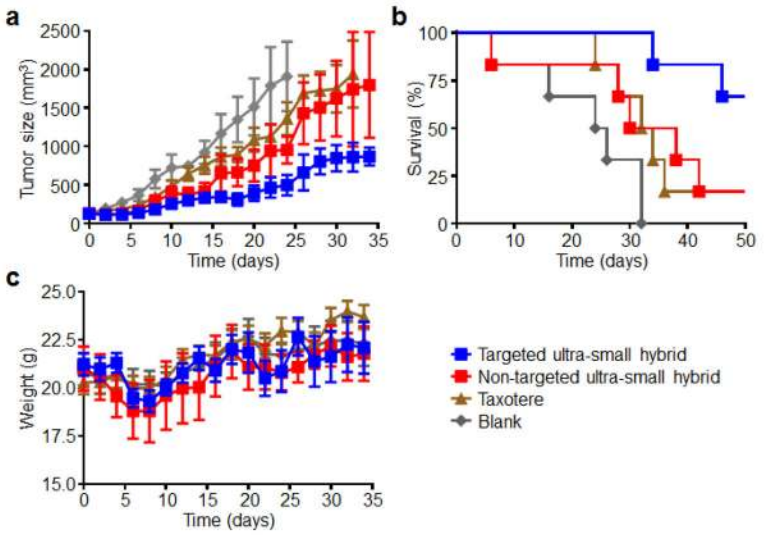

Fig. 7.

In vivo tumor treatment using drug-loaded ultra-small hybrid nanoparticles. (a) Growth kinetics of KB tumors implanted into nude mice and treated with either blank solution, Taxotere, docetaxel-loaded non-targeted hybrid nanoparticles, or docetaxel-loaded folate receptor-targeted hybrid nanoparticles with 4 total doses (twice a week on weeks 3 and 5) at 4 mg/kg of docetaxel each (n = 6; mean ± SEM). (b) Survival curve of mice in (a). Mice were euthanized when tumor volume exceeded 2,000 mm^3. (c) Body weight measurements of mice in (a) (mean ± SEM). All times on x-axes start with the initiation of treatment, corresponding to 14 days after tumor implantation. *P<0.05, ***P<0.001, log-rank test (compared to targeted ultra-small hybrid group).